Preparation, Characterization and Antimicrobial Properties of Ag_2O Nanoparticles Composited with Reduced Graphene Oxide

Hawra H. Obeed[1], ali Mejbel M. Alkhafaji[2,3], Layth Hayder Hameed kazem Al_Tmamimi[4], *Tabarek Falah Deindee [5], Mohammed Ridha Shaeed Janabi[6]*

[1]*Department of Physics, College of Education for Pure Science, University of Kerbala, Karbala, Iraq*

[2]*Department of Pharmacy, Alamal College for Specialized Medical Sciences,*

Karbala, 56001, Iraq

[3] *Ministry of Education, Directorate General of Education in Holy Karbala, Karbala, Iraq*

[4] *Al-Furat Al-Awsat Technical University /Polytechnic College-Karbala/Mechanical Technologies Engineering Department*

[5] *Department of Physics, College of Science, University of Babylon, Babylon, Iraq*

[6] *University of Babylon,Science for women,Laser Physics,Babylon, Iraq*

[DOI: 10.22068/ijmse.4474]

Abstract

Researchers have increasingly investigated hybrid nanocomposites that mix physical and chemical properties of carbonaceous materials and metal/metal oxides. In this work, a nanocomposite composed of reduced graphene oxide and silver (I) oxide, rGO@Ag_2O, was prepared using ascorbic acid as a green reducing agent. The Ag_2O nanoparticles were synthesized by means of a controlled precipitation process in water. The carbonaceous material of rGO was obtained through a modified Hummers' approach. After being combined with a solvent, the Ag_2O and rGO in ethanol were dried with heat. The resultant nanocomposite was structurally and optically examined using different characterization techniques.

The results showed that GO has been successfully reduced, Ag_2O revealed a crystalline structure, and Ag_2O nanostructures were found on the surface of rGO sheets. Disk diffusion assay was adopted in order to evaluate antibacterial activity

of nanocomposite against both *Staphylococcus aureus* (Gram-positive) and *Escherichia coli* (Gram-negative) bacteria. The Ag_2O nanostructures in the composite form exhibited inhibition zone with higher diameter compared to their uncomposited counterparts. Higher antibacterial activity of rGO@Ag_2O was attributed to the role of negatively charged oxygen-containing groups present on the surface of rGO in slightly improvement in the stability of Ag_2O nanostructures.

Our findings show that rGO@Ag_2O could be a useful antimicrobial material for biomedical surfaces, as a coating, and in systems that clean water. It could be a good option for future research in nano-enabled antimicrobial technology because it can destroy bacteria, is made in an environmentally benign way, and could be made on a larger scale.

Keywords: Nanocomposite, Reduced graphene oxide, Silver (I) oxide, Antibacterial activity

1. Introduction

The emergence and rapid dissemination of antibiotic-resistant microorganisms have become a critical global health concern. The increasing prevalence of resistant bacterial strains significantly reduces the effectiveness of conventional antibiotics and highlights the urgent need for alternative antimicrobial strategies. In recent years, nanomaterials—particularly those derived from carbon-based platforms and metal oxides—have attracted considerable scientific interest due to their distinctive physicochemical properties and their capacity to exert broad-spectrum antibacterial effects through mechanisms that differ from those of traditional antimicrobial agents [1, 2].

Among carbon-based nanostructures, graphene oxide (GO) and its derivative, reduced graphene oxide (rGO), have been widely explored for antimicrobial

[DOI: 10.22068/ijmse.4474]

applications. Graphene oxide possesses a two-dimensional carbon framework enriched with oxygen-containing functional groups, including hydroxyl, epoxide, and carboxyl groups. These surface functionalities not only enhance its dispersibility in aqueous environments but also play an important role in antibacterial activity. Previous studies have shown that GO can inhibit bacterial growth through several mechanisms, including physical disruption of bacterial membranes, induction of oxidative stress, and physical immobilization of microbial cells on its surface [3-5].

Despite these advantageous features, the antibacterial performance of GO may be limited by certain intrinsic properties, particularly its relatively low electrical conductivity and its tendency to aggregate under physiological or biological conditions. Reduced graphene oxide (rGO), which contains a lower density of oxygen-containing functional groups, exhibits improved electrical conductivity and a more restored graphitic structure. These characteristics can facilitate stronger interactions with bacterial cell membranes while maintaining essential surface properties required for antimicrobial activity. Nevertheless, when employed individually, both GO and rGO do not always provide sufficiently high bactericidal efficiency, especially against structurally robust Gram-positive bacterial strains, which possess thicker and more complex cell wall structures [6-8].

To further enhance antibacterial performance, recent investigations have focused on the integration of graphene-based materials with metal or metal oxide nanoparticles, enabling the development of hybrid nanostructures that exhibit synergistic antimicrobial mechanisms. Such combinations can simultaneously promote several bactericidal pathways, including the generation of reactive oxygen species (ROS) and the controlled release of antimicrobial metal ions. Within this context, silver(I) oxide (Ag_2O) nanoparticles have attracted particular interest due to their broad-spectrum antibacterial activity, favorable biocompatibility, and comparatively

[DOI: 10.22068/ijmse.4474]

lower cytotoxicity relative to conventional metallic silver nanoparticle [9, 10]. The antibacterial activity of Ag_2O is primarily attributed to the gradual release of Ag^+ ions, which interfere with essential cellular processes by disrupting DNA replication, inactivating key metabolic enzymes, and altering the structural integrity of bacterial cell membranes. In addition, Ag_2O can promote intracellular ROS generation, further intensifying oxidative stress and ultimately reducing bacterial viability [3, 4, 11].

The integration of rGO with Ag_2O nanoparticles into a single nanocomposite system has been reported to produce significantly enhanced antimicrobial performance compared with the individual components. In such hybrid structures, rGO sheets provide a high-surface-area conductive scaffold that facilitates efficient charge transport and promotes the uniform dispersion of Ag_2O nanoparticles across the carbon framework. This structural configuration contributes to a more stable and controlled release of Ag^+ ions. Concurrently, the intrinsic antibacterial activity of Ag_2O, driven by both oxidative processes and ion-mediated interactions, further strengthens the overall antimicrobial response. The combined effects of these components promote improved membrane interaction, metabolic disruption, and ultimately bacterial inactivation. Consequently, several studies have reported that rGO–Ag_2O nanocomposites exhibit substantially larger inhibition zones and lower minimum inhibitory concentrations (MICs) against both Gram-negative and Gram-positive bacterial strains compared with the corresponding individual materials [12-15].

Another notable advantage of such nanocomposite systems is their potential to reduce the likelihood of bacterial resistance development. Unlike conventional antibiotics, which typically target specific cellular pathways, nanocomposites exert antimicrobial activity through multiple concurrent mechanisms. These mechanisms

[DOI: 10.22068/ijmse.4474]

may include physical disruption of bacterial cell structures, induction of oxidative stress, and ion-mediated interactions with essential cellular components. The presence of multiple bactericidal pathways makes it considerably more difficult for microorganisms to develop adaptive resistance over time. Furthermore, the use of rGO as a supporting scaffold allows for a more efficient utilization of silver species, thereby reducing the overall silver content required to achieve effective antibacterial performance. This reduction is particularly important in addressing concerns related to cytotoxicity and the potential environmental accumulation associated with silver-based antimicrobial agents [3, 16].

In parallel with efforts to improve antimicrobial efficiency, recent studies have increasingly emphasized the development of environmentally benign synthesis strategies for rGO–Ag_2O nanocomposites. Various green and sustainable approaches, including plant-extract-mediated synthesis and solvent-free mixing techniques, have been explored to minimize environmental impact and facilitate scalable production. These methods typically avoid the use of hazardous surfactants or stabilizing agents and instead rely on relatively safe solvents, such as ethanol, along with mild reducing agents, including ascorbic acid, to promote nanoscale composite formation. Despite these advances, a comprehensive understanding of the interfacial interactions between rGO and Ag_2O remains limited. In particular, further investigation is required to clarify how these interactions influence the structural characteristics, physicochemical properties, and functional behavior of the resulting nanocomposites under different conditions [16-18].

In the present study, a green and straightforward synthesis approach is proposed for the preparation of an rGO@Ag_2O nanocomposite, in which ethanol is employed as the solvent to facilitate the mixing of the precursor materials. This solvent-mediated strategy promotes the uniform distribution of Ag_2O nanoparticles across the rGO

[DOI: 10.22068/ijmse.4474]

surface while simultaneously supporting the formation of strong interfacial interactions between the rGO sheets and Ag_2O domains.

Following the synthesis process, the structural and optical properties of the rGO@Ag_2O nanocomposite are systematically investigated using several complementary characterization techniques, including X-ray diffraction (XRD), Fourier-transform infrared (FTIR) spectroscopy, Raman spectroscopy, field-emission scanning electron microscopy (FESEM), energy-dispersive X-ray spectroscopy (EDXS), UV–visible (UV–Vis) spectroscopy, and photoluminescence (PL) analysis. In addition, zeta potential measurements are conducted to evaluate the colloidal stability of the nanocomposite after the compositing process, as this parameter plays a critical role in maintaining the effective dispersion of Ag_2O nanoparticles on the rGO surface.

Finally, the antibacterial performance of the synthesized rGO@Ag_2O nanocomposite is assessed through disk diffusion assays against Escherichia coli (E. coli) and Staphylococcus aureus (S. aureus), representing Gram-negative and Gram-positive bacterial strains, respectively. The findings of this study are expected not only to demonstrate the effectiveness of a green solvent-assisted route for the fabrication of rGO-based nanocomposites, but also to provide further insight into how the compositing process influences the antibacterial performance of Ag_2O nanoparticles by improving their dispersion and interaction with carbon-based substrates.

2. Experimental methodology

2-1. Materials

All reagents used throughout this research were of analytical grade and used as received without further purification. Silver nitrate ($AgNO_3$, purity ≥99.8%) and

[DOI: 10.22068/ijmse.4474]

sodium hydroxide (NaOH, pellet form, ≥98%) were procured from Sigma-Aldrich and served as the key precursors for the fabrication of Ag_2O nanoparticles. Graphene oxide (GO) was synthesized from natural graphite powder (≥99.5%, 325 mesh) supplied from Merck, following a modified version of the well-established Hummers' method. Reduced graphene oxide (rGO) was subsequently obtained *via* the chemical reduction of GO using ascorbic acid (≥99%, Alfa Aesar), selected for its environmentally benign reducing capabilities. Ethanol (absolute, ≥99.9%) was used as the dispersing and washing medium during nanocomposite processing. Deionized water was used for all experimental procedures.

2-2. Synthesis of Ag_2O nanoparticles

Silver (I) oxide nanoparticles were prepared using a straightforward aqueous precipitation route adapted from Laouini et al. (2021) [19]. In a typical synthesis, 0.5 gr of $AgNO_3$ were dissolved in 50 mL of deionized water under continuous magnetic stirring. A freshly prepared 0.2 M NaOH solution was then added dropwise until a brown-black precipitate began to form, indicating the generation of Ag_2O. The reaction mixture was maintained under stirring at ambient temperature for two hours to allow for complete precipitation. The resultant solid was separated via centrifugation, washed multiple times with ethanol and deionized water to eliminate residual ions, and subsequently dried in a vacuum oven at 60 °C for 12 hours. This method offers control over nanoparticle morphology and size distribution without resorting to toxic stabilizers or surfactants.

2-3. Synthesis of rGO

To synthesize rGO, graphene oxide was first prepared via a modified Hummers' oxidation of graphite using a combination of concentrated sulfuric acid (H_2SO_4), potassium permanganate ($KMnO_4$), and sodium nitrate ($NaNO_3$), in accordance with the protocol reported by Gebreegziabher et al. (2019) [20]. As-prepared GO was

[DOI: 10.22068/ijmse.4474]

then dispersed in deionized water and subjected to ultrasonic treatment for 30 minutes to exfoliate the layered structure. For the reduction step, 100 mg of GO was mixed with ascorbic acid in a 1:2 mass ratio (GO:AA) and heated to 90 °C with constant stirring for two hours. During the course of the reaction, the suspension gradually changed color from light brown to deep black, signifying successful reduction to rGO. The final product was filtered, thoroughly rinsed with water and ethanol, and dried at 60 °C overnight.

2-4. Synthesis of rGO@Ag_2O nanocomposite

The hybrid rGO@Ag_2O nanocomposite was assembled via a solvent-assisted physical mixing technique. In this process, 0.2 gr of pre-synthesized Ag_2O nanoparticles were suspended in 70 mL of absolute ethanol. Then, 0.1 gr of rGO powder were added to the dispersion. The mixture underwent ultrasonic agitation for 15 minutes to achieve uniform dispersion, followed by magnetic stirring at room temperature for an additional two hours. After blending, the solvent was evaporated under ambient conditions. The resulting solid was dried in a hot air oven at 70 °C for six hours, yielding a fine powder form of the nanocomposite.

2-5. Characterization tests

The structural, compositional, morphological, and optical characteristics of the synthesized samples were examined using an array of analytical techniques. XRD analysis was employed to identify crystallographic phases and estimate crystallite sizes. In order to calculate crystallite size of the bare Ag_2O nanostructures and their nanocomposites with rGO, Debye–Scherrer's equation (Equation 1) was adopted, which is as follows [21, 22]:

$$(1)\quad D = \frac{K\lambda}{\beta cos\theta}$$

[DOI: 10.22068/ijmse.4474]

Where D indicates the mean size, *K* demonstrates the Scherrer constant with the value of 0.98, λ signifies the X-ray wavelength having the value of 1.541 Å, θ is pertinent to Bragg's diffraction angle, and β is related to the full width at half maximum (FWHM).

FTIR spectroscopy was hired to scrutinize organic and inorganic bonds within our samples. The measurements were conducted in the wavenumber varying from 400 to 4000 cm^{-1} using Bruker Tensor 27 spectrophotometer. Surface morphology was studied *via* FESEM test (MIRA3 TESCAN), while elemental composition was assessed through EDXS analysis. The UV-Vis spectroscopy was done by means of Shimadzu UV-2600 instrument. Additionally, PL spectra were recorded using a PerkinElmer LS 55 spectrometer to investigate.

Disk diffusion test or agar diffusion test was conducted in order to study antibacterial activities of rGO, Ag_2O, and rGO@Ag_2O. The measurements were performed for two types of bacteria, including *E.coli* and *S. aureus*. The size of zone of inhibition determines susceptibility degree of the bacterium to antibacterial agent.

3. Results and discussion

3.1. Characterization analysis

Figure 1 demonstrates XRD patterns of rGO, Ag_2O, and rGO@Ag_2O. As evidenced by XRD pattern of rGO (Figure 1), two pronounced diffraction peaks can be found at approximately 26.7 and 42.3 degrees, which correspond respectively to crystal planes of (002) and (100) of rGO [20, 23].

[DOI: 10.22068/ijmse.4474]

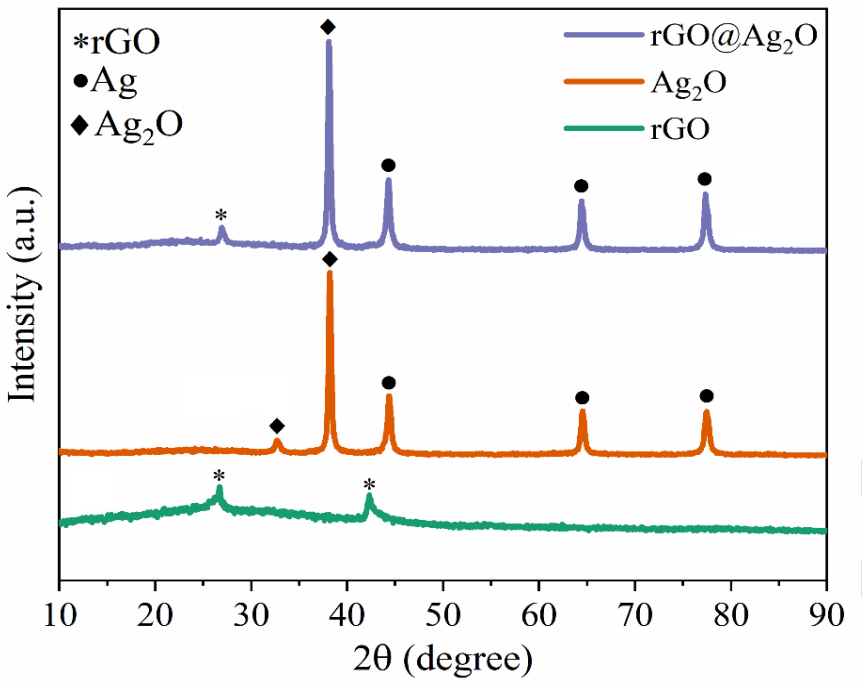

Figure 1. XRD patterns of rGO, Ag_2O, and rGO@Ag_2O.

In addition to rGO, XRD pattern of Ag_2O nanoparticles is depicted in Figure 1. Accordingly, based on JCPDS file No. 01-076-1393, the diffraction peaks located at about 32.85 and 38.2° pertain to (111) and (200) Miller indexes of silver oxide, exhibiting that the prepared Ag_2O nanostructures own the cubic structure [10,19]. Apart from diffraction peaks relevant to Ag_2O, other peaks can be seen, which are situated at 44.4, 64.5, and 77.6°. These peaks are indexed to Miller indexes of (200), (220), and (311), indicating face-centered cubic (*fcc*) structure of Ag (JCPDS file No. 04–0783,) [24-27]. As the XRD pattern of Ag_2O demonstrates, it is the co-existence of both Ag and Ag_2O. Moreover, no peaks other than the ones seen for Ag and Ag_2O can be found, meaning that our sample possesses high purity.

XRD pattern of nanocomposite of rGO@Ag_2O is brought in Figure 1. In this direction, the peak revealing the presence of rGO is detectable at ~26.75°. Besides, the peak exhibiting Ag_2O at 38.1° and the peaks showing Ag at 44.3, 64.45, and 77.3° are observed. The crystallite size calculation for Ag_2O and its nanocomposite

[DOI: 10.22068/ijmse.4474]

was carried out using Equation 1. In this regard, the values obtained for Ag_2O and rGO@Ag_2O respectively were 36.02 nm and 37.17 nm.

FTIR spectrum of rGO is illustrated in Figure 2a. Accordingly, the wide FTIR peak seen at about 3394 cm^{-1} is associated with the stretching vibration of hydroxyl (-OH) group, which is arisen from H_2O molecules and carboxylic acids [17, 28, 29].

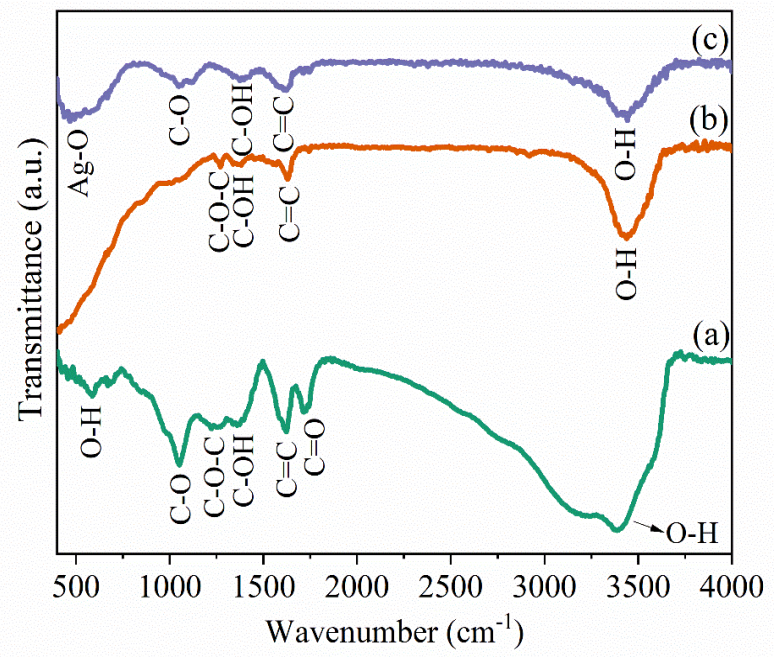

Figure 2. FTIR spectra of (a) rGO, (b) Ag_2O, and (c) rGO@Ag_2O.

The absorption band evident at 1716 cm^{-1} corresponds to carbonyl (C=O) available in carboxylic groups (-COOH), which are commonly found at the edges of GO sheets. The sharp FTIR peak at 1623 cm^{-1} pertains to sp^2 vibration plane of C=C double bonds [17,28,29]. The peak situated at 1373 cm^{-1} is related to bending vibration of hydroxyl (C-OH) groups and the peak centered at 1224 cm^{-1} is ascribed to the bending vibration of epoxy (C-O-C) groups. The absorption band at the wavenumber of 1058 cm^{-1} signifies stretching vibration of C-O bond in ether, epoxy, or peroxide groups. In addition, the FTIR peak at 588 cm^{-1} is associated with out-of-plane bending vibration of –OH group [17,28,29]. Figure 2b demonstrates FTIR

[DOI: 10.22068/ijmse.4474]

spectrum of Ag_2O nanostructures. In this regard, the peaks demonstrating the functional groups appeared as a result of green fabrication of silver oxide are apparent. The absorption band centered at 3436 cm^{-1} exhibiting stretching vibration of O-H bond is clearly observed. The FTIR peak found at 1625 cm^{-1} is associated with C=C double bond. The peaks at 1382 cm^{-1} related to bending vibration of hydroxyl (C-OH) and at 1272 cm^{-1} relevant to epoxy (C-O-C) are detectable. In accordance with literature, the FTIR peaks demonstrating metal–oxygen bonds commonly emerge in the range of 400 to 800 cm^{-1}, located in fingerprint region [30-32]. Accordingly, no noticeable absorption band attesting the presence of Ag-O peak can be seen in the aforementioned range. FTIR spectrum of rGO@Ag_2O nanocomposite is brought in Figure 2c. Apart from absorption bands related to rGO and the ones detected in Figure 2b, a wide peak is perceptible in the range of 400 to 800 cm^{-1}, which is ascribed to Ag-O-Ag bonds.

FESEM images of our samples are brought in Figure 3. In agreement with Figure 3a exhibiting FESEM image of rGO, the flakes of this carbonaceous material are evident, which have layered structure and full of folding and wrinkles are seen on their surface. Figure 3b exhibits FESEM image of Ag_2O nanoparticles. In this regard, agglomerated spherical and also polygonal-shaped nanostructures of Ag_2O are detectable, which are evenly dispersed. As confirmed by the FESEM image of rGO@Ag_2O nanocomposite (Figure 3c), the agglomerated round and polygonal-shaped nanoparticles of silver oxide are seen, which are found on the surface of rGO.

[DOI: 10.22068/ijmse.4474]

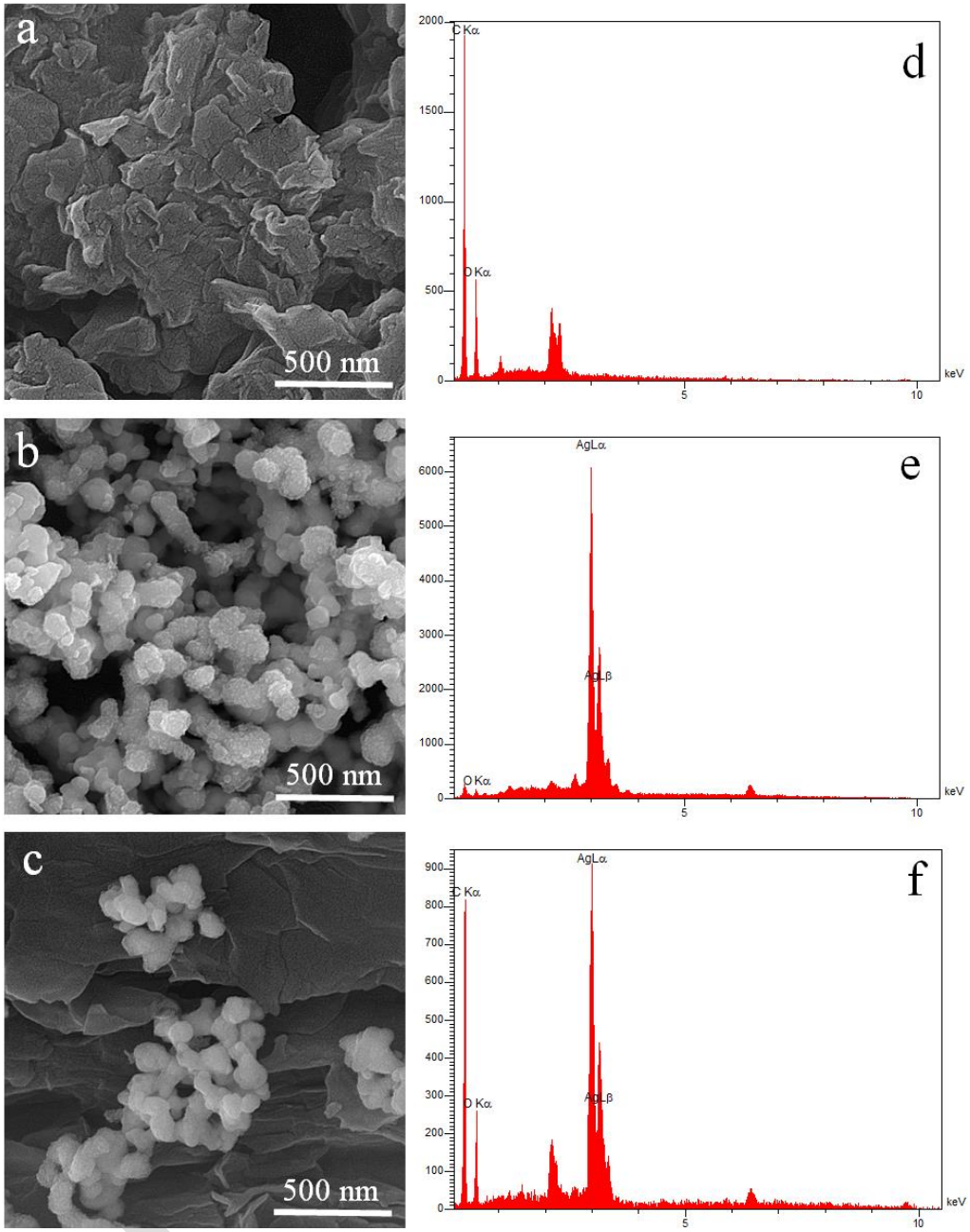

Figure 3. (a,b,c) FESEM images of rGO, Ag_2O, and rGO@Ag_2O, respectively. (d,e,f,) EDXS patterns of rGO, Ag_2O, and rGO@Ag_2O, respectively.

Based on EDXS pattern of rGO (Figure 3d), the peaks of carbon (C) and oxygen (O) are conspicuous separately at 0.25 and 0.5 keV, which are originated from this material. EDXS pattern of Ag_2O nanoparticles appear in Figure 3e. To this end, the pronounced peaks of silver (Ag) emerge at approximately 3.0 and 3.25 keV. In

[DOI: 10.22068/ijmse.4474]

addition, the peak of oxygen element is seen at 0.5 keV. The aforementioned peaks are arisen from Ag_2O. As evidenced by EDXS pattern of rGO@Ag_2O composite (Figure 3f), the peaks of C and O elements related to rGO and also the peaks of O and Ag pertinent to Ag_2O can be observed.

Figure 4 exhibits Raman spectra of rGO, Ag_2O, and rGO@Ag_2O. As evidenced by Raman spectrum of rGO, two attenuated peaks can be observed, one of which is located at 1279 cm^{-1} and the other is found at 1513 cm^{-1}. The peak centered at 1279 cm^{-1} is related to D-band, which signifies sp^3 defects inside the structure of rGO. Valuable information regarding defects on surface of carbonaceous material and also structural imperfections within it can be perceived from D-band. This band owns the symmetry of A_{1g} and manifests breathing mode of k point phonons [33-36]. In addition to the peak at 1279 cm^{-1}, another peak is detectable at 1513 cm^{-1}, which is associated with G-band. The vibrational mode of E_{2g} belongs to this band. G-band is an indication of in-plane vibration of sp^2 carbon atoms whose symmetry and also crystallizability can be investigated by this band [33-36].

In the Raman spectrum of Ag_2O (Figure 4), several peaks are seen, which are located at 116, 183, 296, 386, 489, and 1193 cm^{-1}. In the Raman spectrum of rGO@Ag_2O nanocomposite, the peaks showing rGO and Ag_2O are evident. In this regard, the peaks exhibiting D-band and G-band are respectively centered at 1269 and 1487 cm^{-1}. Moreover, the peak at 489 cm^{-1} relevant to Ag_2O shifts to 577 cm^{-1}. The shift in the position of the peak could be an evidence for chemical bonding between Ag_2O nanostructures and rGO sheets [35]. The broad peak appears at 2990 cm^{-1} is ascribed to *2D* band of rGO [37].

[DOI: 10.22068/ijmse.4474]

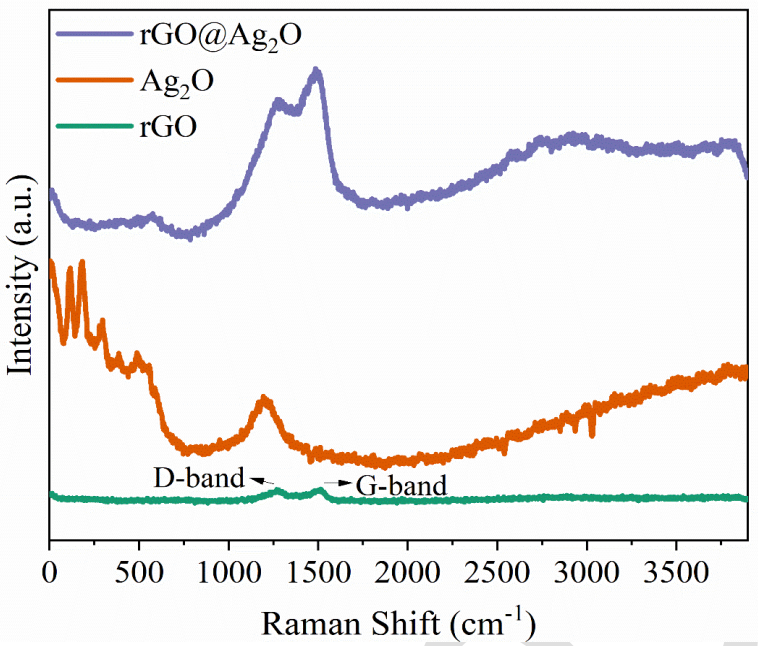

Figure 4. Raman spectra of rGO, Ag_2O, and rGO@Ag_2O.

Figure 5 exhibits zeta potentials of synthesized rGO, Ag_2O, and rGO@Ag_2O. Moreover, the mean zeta potentials obtained for the abovementioned samples are listed in Table 1.

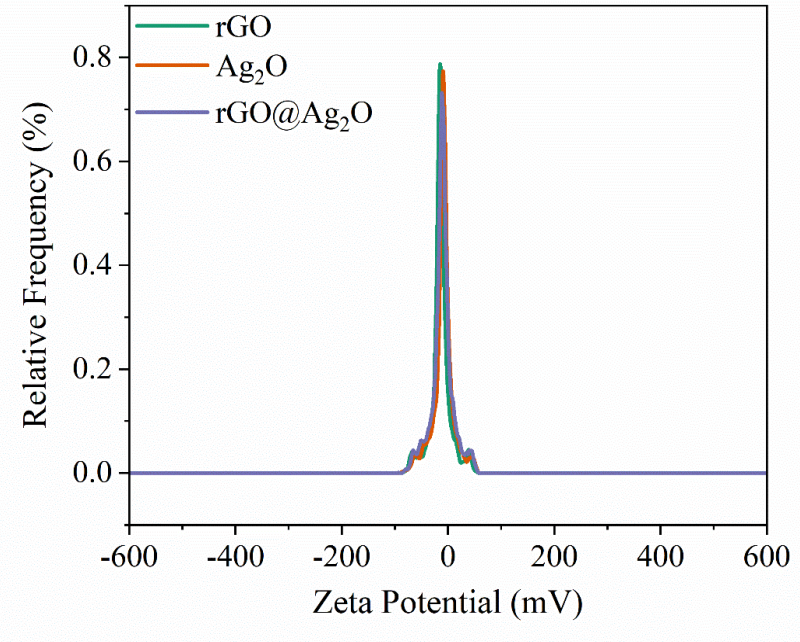

Figure 5. Zeta potentials of rGO, Ag_2O, and rGO@Ag_2O.

[DOI: 10.22068/ijmse.4474]

Zeta potential is a beneficial factor for measuring stability of rGO, Ag_2O, and rGO@Ag_2O in a dispersion for instance suspensions. It determines the electrical charge present on the surface of particles [38].

Table 1. Mean zeta potentials of rGO, Ag_2O, and rGO@Ag_2O.

Sample	Mean zeta potential (mV)
rGO	-13.6
Ag_2O	-9.3
rGO@Ag_2O	-11.2

According to Table 1, the zeta potential obtained for rGO flakes is -13.6 mV. Based on literature, the zeta potential of GO and rGO is arisen from the existence of negatively charged oxygen-containing groups, like hydroxyl, carboxyl and epoxy, on their surface [16, 39]. Compared to rGO, Ag_2O nanostructures reveal less zeta potential. Accordingly, the zeta potential seen for this sample is -9.3 mV. The zeta potential acquired for rGO@Ag_2O composite is -11.2 mV, implying that compositing Ag_2O nanoparticles with rGO resulted in a slightly increment in their zeta potential, which can be attributed to the role of negatively charged oxygen-containing groups present on rGO.

3.2. Antibacterial activities assay

According to Figure 6a and antibacterial activity of rGO, the zone of inhibition shows negligible diameter, implying that rGO demonstrates little activity against *E. coli* bacteria. On the other hand, the size of diameter of inhibition zone seen for Ag_2O is more than the one seen for rGO. The rGO@Ag_2O nanocomposite reaches inhibition zone with highest diameter among all the prepared samples, meaning that it is more efficient against *E. coli* bacteria compared to Ag_2O and rGO.

[DOI: 10.22068/ijmse.4474]

Figure 6b illustrates antibacterial activity of synthesized samples against *S. aureus*. In this regard, no inhibition zone is observed for rGO, implying that this sample shows no antibacterial activity against *S. aureus*. On the other hand, a zone of inhibition with negligible diameter is detectable for Ag_2O. By compositing Ag_2O nanostructures with rGO, an improvement occurred in their antibacterial activity against *S. aureus*.

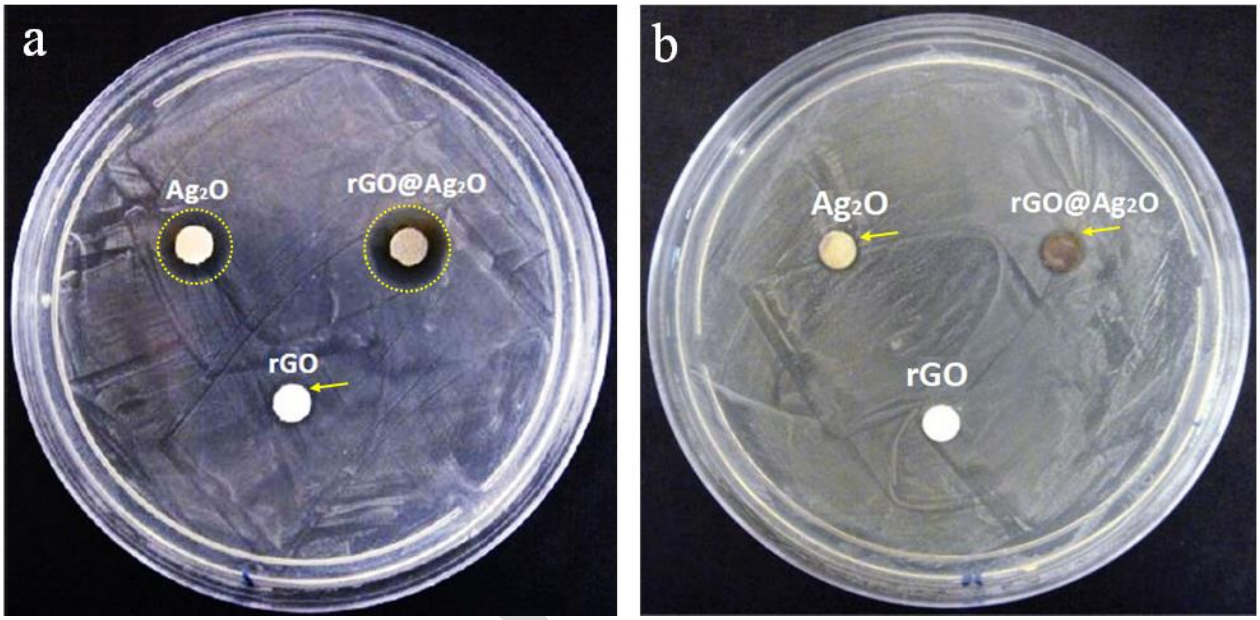

Figure 6. Antibacterial activities of prepared samples against (a) *E. coli* and (b) *S. aureus* bacteria.

In some literature, the better antibacterial activity of rGO@Ag_2O compared to each of its constituents was ascribed to higher number of produced Ag^+ ions and also reactive oxygen species compared to each of rGO and Ag_2O, which results in a disrupting interaction with bacteria's wall through membrane proteins [7]. However, the results obtained from this study revealed that increased stability of Ag_2O nanostructures ensuing from compositing process could be another reason for improving their antibacterial activity. Accordingly, although rGO possesses negligible antibacterial activity, it slightly increases stability of Ag_2O nanostructures through it negatively charged oxygen-containing groups. In other words and

[DOI: 10.22068/ijmse.4474]

alongside its role in providing a support matrix for Ag_2O nanostructures, rGO could act as a dispersing agent, which is a critical factor for distribution of Ag_2O nanostructures and subsequently, improving their antibacterial activity.

4. Conclusions

In the current study, rGO@Ag_2O composites were synthesized in order to examine their antibacterial activity against gram-negative and gram-positive bacteria. In the XRD pattern of rGO@Ag_2O nanocomposite, in addition to peak related to rGO, the peaks of Ag and Ag_2O appeared. The morphology seen for the nanocomposite was a combination of singly Ag_2O and rGO. As evidenced by FESEM image of nanocomposite, agglomerated spherical and polygonal-shaped Ag_2O nanostructures dispersed on the surface of rGO flakes were detected.

Compositing Ag_2O nanoparticles with rGO not only increased slightly their stability, but also improved their antibacterial activity. rGO showed negligible antibacterial activity; but, the presence of charged oxygen-containing groups on its surface resulted in an insignificant increment in the stability of Ag_2O nanostructures. Our research points out that carbonaceous materials like rGO not only could appear as a support matrix for metal/metal oxide nanoparticles, but also act as a dispersing agent, which is essential for distribution of metal/metal oxide nanoparticles and their antibacterial activity.

References

1. Chaudhary, R., et al., Antibacterial activity of reduced graphene-silver oxide nanocomposite against gram-negative bacteria. The Microbe, 2024. 5: p. 100221.
2. Sreeprasad, T.S., et al., Reduced graphene oxide–metal/metal oxide composites: facile synthesis and application in water purification. Journal of hazardous materials, 2011. 186(1): p. 921-931.

[DOI: 10.22068/ijmse.4474]

3. Gautam, A., et al., Graphene-based metal/metal oxide nanocomposites as potential antibacterial agents: a mini-review. Biomaterials Science, 2024.
4. Sharma, R., et al., Synergistic advancements in nanocomposite design: Harnessing the potential of mixed metal oxide/reduced graphene oxide nanocomposites for multifunctional applications. Journal of Energy Storage, 2024. 93: p. 112317.
5. Hossain, K., et al., Antimicrobial activity of graphene-based nanomaterials: Current development and challenges, in Graphene-Based Nanotechnologies for Energy and Environmental Applications. 2019, Elsevier. p. 293-314.
6. Liu, S., et al., Antibacterial activity of graphite, graphite oxide, graphene oxide, and reduced graphene oxide: membrane and oxidative stress. ACS nano, 2011. 5(9): p. 6971-6980.
7. Sajjad, S., et al., GO/Ag_2O composite nanostructure as an effective antibacterial agent. ChemistrySelect, 2019. 4(35): p. 10365-10371.
8. Zheng, H., et al., Engineered graphene oxide nanocomposite capable of preventing the evolution of antimicrobial resistance. ACS nano, 2019. 13(10): p. 11488-11499.
9. Wadhwa, H., et al., Microwave assisted facile synthesis of reduced graphene oxide-silver (RGO-Ag) nanocomposite and their application as active SERS substrate. Materials Chemistry and Physics, 2017. 194: p. 274-282.
10. Fayyadh, A.A. and M.H. Jaduaa Alzubaidy, Green-synthesis of Ag_2O nanoparticles for antimicrobial assays. Journal of the Mechanical Behavior of Materials, 2021. 30(1): p. 228-236.
11. Vi, T.T.T., et al., Synergistic antibacterial activity of silver-loaded graphene oxide towards Staphylococcus aureus and Escherichia coli. Nanomaterials, 2020. 10(2): p. 366.
12. Bellier, N., et al., Recent biomedical advancements in graphene oxide-and reduced graphene oxide-based nanocomposite nanocarriers. Biomaterials research, 2022. 26(1): p. 65.
13. Bai, R.G., et al., The biogenic synthesis of a reduced graphene oxide–silver (RGO–Ag) nanocomposite and its dual applications as an antibacterial agent and cancer biomarker sensor. RSC advances, 2016. 6(43): p. 36576-36587.

[DOI: 10.22068/ijmse.4474]

14. Murugan, S., et al., Green synthesis of Ag_2O/ZnO nanocomposite for efficient antibacterial property and tunable electrochemical detection of hydrogen peroxide. Journal of Environmental Chemical Engineering, 2025. 13(3): p. 116394.
15. Jose, P.P.A., et al., Reduced graphene oxide/silver nanohybrid as a multifunctional material for antibacterial, anticancer, and SERS applications. Applied physics A, 2020. 126(1): p. 58.
16. Roy, I., et al., Physical and electrochemical characterization of reduced graphene oxide/silver nanocomposites synthesized by adopting a green approach. RSC Advances, 2015. 5(32): p. 25357-25364.
17. Faniyi, I., et al., The comparative analyses of reduced graphene oxide (RGO) prepared via green, mild and chemical approaches. SN Applied Sciences, 2019. 1: p. 1-7.
18. Sharma, N., et al., A comparative study on gas-sensing behavior of reduced graphene oxide (rGO) synthesized by chemical and environment-friendly green method. Applied Nanoscience, 2020. 10: p. 517-528.
19. Laouini, S.E., et al., Green synthesized of Ag/Ag_2O nanoparticles using aqueous leaves extracts of Phoenix dactylifera L. and their azo dye photodegradation. Membranes, 2021. 11(7): p. 468.
20. Gebreegziabher, G., et al., One-step synthesis and characterization of reduced graphene oxide using chemical exfoliation method. Materials Today Chemistry, 2019. 12: p. 233-239.
21. Arshad, J.M., et al., Synthesis and characterization of cobalt ferrites as MRI contrast agent. Materials Today: Proceedings, 2021. 47: p. S50-S54.
22. Meena, P.L., et al., Ag_2O-adorned ZnO nanostructures: cooperative and sustainable nanomaterial system for effective reduction and mineralization of hazardous water pollutants. Environmental Science and Pollution Research, 2023. 30(26): p. 68770-68791.
23. Jayachandiran, J., et al., Synthesis and electrochemical studies of rGO/ZnO nanocomposite for supercapacitor application. Journal of Inorganic and Organometallic Polymers and Materials, 2018. 28: p. 2046-2055.
24. Thangamani, N. and N. Bhuvaneshwari, Synthesis, characterization of Ag nanoparticles using the green approach towards degradation of environmental pollutant. Journal of Materials Science: Materials in Electronics, 2022. 33(12): p. 9155-9162.

[DOI: 10.22068/ijmse.4474]

25. Lee, J.-W., et al., Synthesis of silver nanoparticles embedded with single-walled carbon nanotubes for printable elastic electrodes and sensors with high stability. Scientific Reports, 2021. 11(1): p. 5140.
26. Kalaivani, R., et al., Synthesis of chitosan mediated silver nanoparticles (Ag NPs) for potential antimicrobial applications. Frontiers in Laboratory Medicine, 2018. 2(1): p. 30-35.
27. Sarkar, S. and R. Das, Shape effect on the elastic properties of Ag nanocrystals. Micro & Nano Letters, 2018. 13(3): p. 312-315.
28. Jayanti, P.D., et al., Localized surface plasmon resonance properties of green synthesized Ag/rGO composite nanoparticles utilizing Amaranthus viridis extract for biosensor applications. Journal of Science: Advanced Materials and Devices, 2024. 9(3): p. 100747.
29. Ruidíaz-Martínez, M., et al., Hydrothermal synthesis of rGO-TiO2 composites as high-performance UV photocatalysts for ethylparaben degradation. Catalysts, 2020. 10(5): p. 520.
30. Pasieczna-Patkowska, S., M. Cichy, and J. Flieger, Application of Fourier Transform Infrared (FTIR) Spectroscopy in Characterization of Green Synthesized Nanoparticles. Molecules, 2025. 30(3): p. 684.
31. Chen, J., et al., A sustainable chrome-free tanning approach based on Zr-MOFs functionalized with different metals through post-synthetic modification. Chemical Engineering Journal, 2023. 474: p. 145453.
32. Scaria, S.S. and K.S. Joseph, Exploring the photocatalytic and cytotoxic potential of quassia indica-derived bimetallic silver-zinc oxide nanocomposites. Waste and Biomass Valorization, 2024. 15(11): p. 6251-6265.
33. Scardaci, V. and G. Compagnini, Raman spectroscopy investigation of graphene oxide reduction by laser scribing. C, 2021. 7(2): p. 48.
34. Das, P., A.B. Deoghare, and S.R. Maity, A novel approach to synthesize reduced graphene oxide (RGO) at low thermal conditions. Arabian Journal for Science and Engineering, 2021. 46(6): p. 5467-5475.
35. Khan, M.A., et al., Enhanced antibacterial and visible light driven photocatalytic activity of graphene oxide mediated Ag 2 O nanocomposites. Optical and Quantum Electronics, 2024. 56(9): p. 1422.

[DOI: 10.22068/ijmse.4474]

36. Tran, D.T., rGO/persulfate metal-free catalytic system for the degradation of tetracycline: effect of reaction parameters. Materials Research Express, 2020. 7(7): p. 075501.
37. Ramli, M.M., et al., Cell viability and electrical response of breast cancer cell treated in aqueous graphene oxide solution deposition on interdigitated electrode. Scientific Reports, 2021. 11(1): p. 20702.
38. Landi, S., et al., Functionalization of cotton by RGO/TiO 2 to enhance photodegradation of rhodamine B under simulated solar irradiation. Water, Air, & Soil Pollution, 2017. 228: p. 1-16.
39. Mindivan, F., The synthesis and charecterization of graphene oxide (GO) and reduced graphene oxide (rGO). Machines. Technologies. Materials., 2016. 10(6): p. 32-35.

[DOI: 10.22068/ijmse.4474]